CEWES MSRC/PET TR/99-22

Coupling of Marine Circulation and Wind-Wave Models on Parallel Platforms

by

D. J. S. Welsh
R. Wang
P. Sadayappan
K. W. Bedford

04h02199

Work funded by the DoD High Performance Computing Modernization Program CEWES Major Shared Resource Center through

Programming Environment and Training (PET)

Supported by Contract Number: DAHC94-96-C0002
Nichols Research Corporation

Coupling of Marine Circulation and Wind-Wave Models on Parallel Platforms

D. J. S. Welsh[1], R. Wang[2], P. Sadayappan[2], and K. W. Bedford[1]

March 26th, 1999

Abstract

Accurate predictions of wave heights, currents, and water elevations are vital inputs in the planning of military operations in the marine environment. Marine circulation and wind-wave models have traditionally been run separately, but recent research has identified potentially important interactions between current and wave motions. This report details the coupling of the CH3D circulation model and the WAM wave model at the atmospheric boundary layer. The MPI parallel CH3D code and the OpenMP parallel WAM code have been coupled on the SGI ORIGIN 2000 at CEWES MSRC. Communication between the models is achieved using MPI. Scalability results are presented for the individual codes and the coupled system. Results are included from Lake Michigan hindcasts. The hindcasts show that wave-current interactions have a significant effect on storm surges and the associated currents. Work has also begun on the coupling of WAM and CH3D-SED, which includes the SED sediment transport model, at the bottom boundary layer. Details of the physics of this coupling are included in this report.

1. Introduction

Marine circulation and wind-waves have traditionally been modeled independently. It has recently been suggested, however, that there can be significant interactions between the two motions (Holthuisen and Tolman, 1991, and Glenn and Grant, 1987, for example). The interactions are typically largest in shallow water and other high current regions. The effects on storm surges, circulation patterns, wave heights, and wave breaking can potentially be a critical factor in the strategic planning of military and national security operations including beach landings, route selection, and search and rescue missions. The aim of this focused effort was to complete the work begun in PET year 2 on the coupling of wave and circulation models at the atmospheric boundary layer (Zhang et al., 1998), and to add performance scalability by moving to parallelized codes and computational platforms. An additional target was to begin the coupling of WAM and the CH3D-SED model at the bottom boundary layer. The SED sub-model predicts sediment transport and concentrations; it is fully integrated with the circulation calculations in CH3D-SED.

[1]The Ohio State University, Department of Civil and Environmental Engineering and Engineering Graphics
[2]The Ohio State University, Department of Computer and Information Science

2. Coupling at the atmospheric boundary layer

2.1 Model descriptions

The CH3D marine circulation model (Chapman et al., 1996) and WAM wind-wave model (WAMDI, 1988) have been used in this focused effort. CH3D predicts the three-dimensional current, temperature, and salinity fields, and the two-dimensional water surface elevation field. The model solves conservation equations for mass, momentum, and thermal energy using finite difference discretizations on a curvilinear horizontal grid and a sigma layer (terrain following) vertical grid. A mode-splitting solution technique is used in which external (barotropic) and internal (baroclinic) motions are solved separately, allowing an enhanced baroclinic time-step. The external mode uses vertically-averaged equations to predict water surface elevations and mean horizontal velocities, then the internal mode re-introduces vertical variations. CH3D requires inputs of time-varying water surface winds and heat fluxes or air temperatures.

The WAM wind-wave model predicts frequency-direction spectra of wave energy on a regular grid; significant wave height, mean wave period, and mean wave direction are calculated from the spectra. WAM cycle 4 (Gunther et al., 1992) is used here. This version is based on the conservation of wave action density and includes advanced, “third-generation” physics (Komen et al., 1994) in the treatment of the wind input, nonlinear wave-wave interaction, and dissipation source terms. WAM includes algorithms for current-induced wave propagation and refraction, and for depth-induced refraction and shoaling. In the basic model, depth and current effects are assumed to be steady throughout a single simulation, but in PET year 2 unsteady current and depth effects were added (Zhang et al., 1998). Model inputs are time-varying surface winds and, optionally, current fields.

CEWES staff supplied parallel versions of CH3D and WAM for use in this focused effort. Both codes use one-dimensional domain decomposition, with the computational grid split into blocks of contiguous rows, and the number of blocks specified by the user. Each block is assigned to a different processor and the Message Passing Interface (MPI) library is used for communication between slave processes and the master process.

The parallel version of CH3D was found to reproduce the predictions of the original, sequential code, but this was not the case with parallel WAM. For the idealized Lake Michigan test described in Zhang et al. (1998), parallel WAM produced wave height errors on the order of 2% at some grid points adjacent to the shoreline. Dr. Robert Jensen of the CEWES Coastal and Hydraulics Laboratory also found larger wave height errors in deep water in a nested-grid simulation of Hurricane Luis. Further investigation showed that the errors in parallel WAM were related to current effects in shallow water and the passing of boundary conditions between nested grids. Due to the errors, MPI-based parallel WAM was replaced by an OpenMP version of the sequential WAM code.

OpenMP allows individual loops in a code to be declared as parallel regions and within that loop multi-processing is performed. If the sequential code is first compiled with the Power Fortran Analyzer (PFA) argument, one can obtain suggestions for OpenMP directives. By trial and error,

one can then determine which suggestions are beneficial. It is best to concentrate such efforts on the most demanding subroutines in a code. This approach was followed with WAM, resulting in the declaration of eight OpenMP regions in the four most time-consuming subroutines: SNONLIN, IMPLSCH, SINPUT, and PROPAGS.

2.2 Coupling strategy and coupling physics

A coupled simulation involving MPI CH3D and OpenMP WAM is launched using the MPI *mpirun* command, with one process specified for WAM and multiple processes specified for CH3D. The WAM process spawns multiple threads in the OpenMP regions, with the number of threads set by the WAM shell script invoked in the *mpirun* command line. MPI is used for communication between the CH3D master process and WAM; their process numbers in the MPI_COMM_WORLD communicator are evident from the *mpirun* command line. Separate communicators are defined for intra-model communication within CH3D, and for inter-model communication. This strategy was used to simplify the planned addition of marine sediment transport and atmospheric circulation models to the coupled system. The frequency of coupling between the models is set in each model's main input file. The coupling time-step must be divisible exactly by each model's propagation time-step.

The formulation of the OpenMP library is based on a shared memory multi-processing architecture, as found on the SGI ORIGIN 2000 (O2K) platform used at CEWES MSRC. All coupling operations in this report have therefore used the O2K, but a version of OpenMP is expected to be available for the IBM SP-2 in 1999. This will introduce portability to the CH3D/WAM coupled system. Cross-platform coupling will also be possible using the MPI_Connect library developed under the PET SPP Tools support area by the University of Tennessee at Knoxville. This library will allow processes to communicate when they are running on different types of platforms at different locations. The PET CFD team at CEWES has verified the operation of MPI_Connect using CG-WAVE harbor wave simulations running at three geographically distant O2K platforms (Bova et al., 1999).

The governing equations of CH3D and WAM are detailed in Zhang et al. (1998) and will not be repeated here. Coupling effects are also described extensively in that reference. In summary, coupling at the atmospheric boundary layer requires the passing of CH3D surface currents and water surface fluctuations to WAM, and the passing of WAM wind stresses and radiation stresses (Phillips, 1977) to CH3D. The effects of waves on currents consist of a modified wind input to the current field due to waves roughening the water surface, plus direct transfer of surface momentum, either positive or negative, by means of the radiation stress tensor. The effects of currents on waves are modified depth-refraction due to time-varying depths, transport of individual waves by local surface current, refraction of waves due to the spatial variation of currents, modified wind input using the effective wind speed, modified bottom friction due to shifted wave frequencies relative to the bed, and delayed or promoted wave breaking. Both wave effects in CH3D were implemented in PET year 2. Wave breaking is not modeled in WAM, but all other current effects on WAM predictions were added in PET year 2, with the exception of modified bottom friction. Please note that this discussion of coupling does not include the wave-current bottom boundary layer, which is addressed in section 3 of this report.

WAM predicts the bottom friction energy dissipation rate for a particular component of the wave energy spectrum using the algorithm of Hasselmann et al. (1973):

$$S_{bf}(\omega,\theta) = \frac{-0.076}{g} \cdot \frac{k}{\sinh kh} E(\omega,\theta), \quad (1)$$

where ω is the radian wave frequency relative to the fixed bed, θ is the wave component's direction, g is gravitational acceleration, k is wavenumber, h is water depth, and $E(\omega,\theta)$ is the wave energy density. The basic version of WAM cycle 4 calculates propagation and source/sink terms in (σ,θ) space, however, where σ is the radian wave frequency relative to the moving frame of reference defined by the surface currents. (At output time-steps WAM interpolates each $E(\omega,\theta)$ from the $E(\sigma,\theta)$ spectra). This means that (1) is used for $S_{bf}(\sigma,\theta)$ and $E(\sigma,\theta)$ without taking account of the relation between ω and σ:

$$\omega = \sigma + \tilde{k} \cdot \tilde{U}, \quad (2)$$

where $\tilde{U}$ is the current vector. In PET year 3 this omission has been rectified. For each wave component, (2) is used to calculate ω; the selected spectral grid fixes the value of σ. A modified value of wavenumber is then obtained from WAM's pre-processed look-up table array, $TFAK(h,\omega)$, and used in (1) with ω replaced by σ. (To save time, $TFAK$ contains pre-computed values of k for a grid of h and ω values; for particular h and ω values, the nearest array element provides an approximate k.)

2.3 Idealized test cases

The idealized test used in Zhang et al. (1998) was re-run after the implementation of the bottom friction coupling. Comparisons of predictions with and without the modified bottom friction algorithm indicated that this coupling has a negligible effect. This finding may be in part due to the coarse resolution of the $TFAK(h,\omega)$ look-up table (52 depths, covering 5 m to 568 m; the same 25 frequencies as the $E(\omega,\theta)$ grid). The lack of impact also suggests that the introduction of a full wave-current boundary layer treatment, as described in section 3 of this report, is necessary for the accurate representation and assessment of wave-current bottom boundary layer interactions.

After the implementation of the modified bottom friction algorithm, the dominant current effect on WAM wave predictions continued to be modified wind input due to the shifted relative motion of the waves and winds. The idealized test in Zhang et al. (1998) found this to alter wave heights on the order of 5 %. It was stated there, however, that in high current situations this percentage could significantly increase. This belief confirmed by the results of a second idealized test performed in PET year 3. This test again used the 3 minutes longitude by 2 minutes latitude (approximately 4-km square cells), 67 x 139 Lake Michigan bathymetry grid. Lake Michigan has been used as a test site due to the simple boundary conditions and availability of data. Idealized test 2 ("I2") used idealized currents, rather than CH3D currents, to more clearly show coupling effects on waves. A no-wave initial condition was used, then a 5 m/s northerly wind was applied

for 24 hours. In test I2A, currents of 0.5 m/s from the north were input to WAM; in test I2B, currents of 0.5 m/s from the south were used. Figures 1 and 2 show the significant wave height contours and wave height-scaled vectors at hour-24 of tests I2A and I2B, respectively.

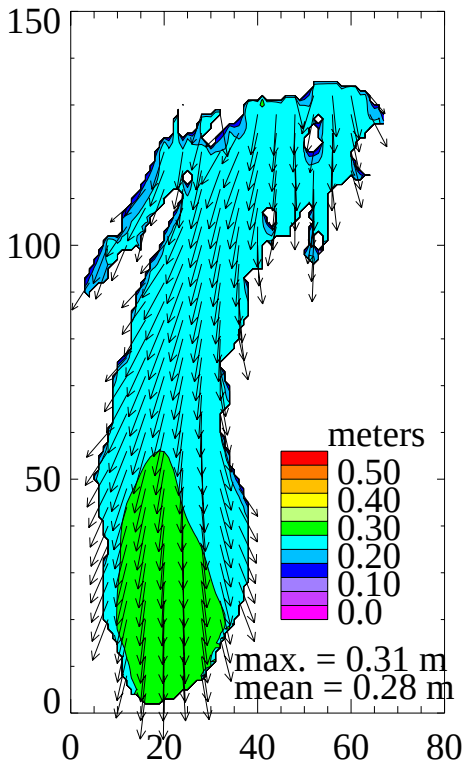

Figure 1: WAM significant wave height contours and vectors at hour-24 of test I2A

Currents which transport waves in a direction opposing winds cause an increased effective wind speed and, therefore, larger waves. This is borne out by the 30 – 40 % larger waves seen in Figure 2, relative to Figure 1. These differences indicate the potential importance of current effects on waves. While the currents in test I2 are not realistic for Lake Michigan, large currents over a wide areal extent can be found in the open ocean; the Gulf Stream is one example of this. It should be noted that the WAM model initially gave larger wave heights in test I2A than in test I2B. This counter-intuitive behavior was traced to sign errors in the main propagation subroutine.

2.4 Lake Michigan hindcasts

The coupling of CH3D and WAM has been evaluated further using Lake Michigan hindcasts. These hindcasts cover a high activity period of the NOAA/NSF “Episodic Events – Great Lakes Environment” (EEGLE) field data collection and analysis project (Schwab et al., 1999). The purpose of the EEGLE project is to observe and model the causes and effects of sediment plume events in southern Lake Michigan. The project involves three years of data collection by means of moored instruments and targeted survey cruises. The data being collected includes current profiles, wave heights, temperatures, sediment concentrations, sediment compositions, pollutant and nutrient levels, drifter GPS paths, and meteorological conditions. The moored instruments are located along five coastal transects offshore of Muskegon, Saugatuck, and St. Joseph, MI;

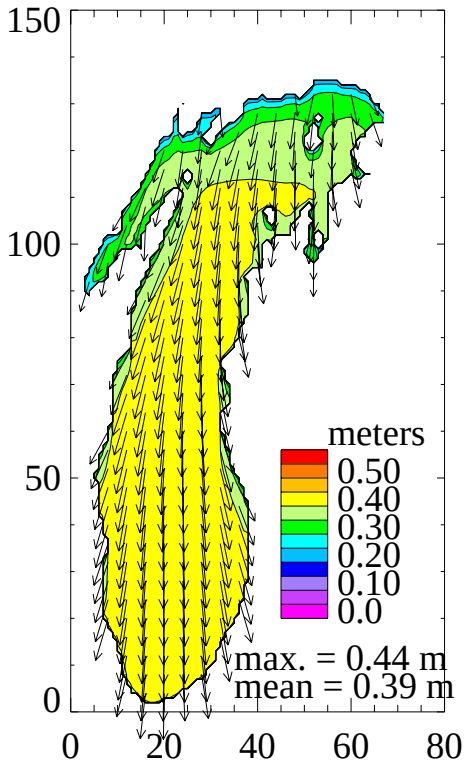

Figure 2: WAM significant wave height contours and vectors at hour-24 of test I2B

Gary, IN; and Racine, WI. In addition to EEGLE instruments, NOAA wave buoys 45002 and 45007 are moored in Lake Michigan from early Spring until late Fall, and NOAA also collects meteorological observations on hourly or three-hourly schedules from some fifty stations around the coast of the lake.

The coupled CH3D and WAM hindcasts analyzed here cover Julian days 86 through 99 (March 27th through April 9th), 1998. This period was selected based on event magnitude and data availability. During the period, satellite imagery indicated that a significant sediment plume developed and buoy data included winds up to 25 knots (13 m/s) and significant wave heights up to 3 m. Coincident and continuous current and wave data were collected at one station in the Racine transect. Conditions were fairly quiescent at day 86, which provided an opportunity for realistic model spin-up.

The basic CH3D model requires surface water temperatures or heat exchange coefficients and equilibrium temperatures as a time-varying boundary condition. Since insufficient temperature data was available for the EEGLE hindcasts, code was added to calculate surface heat flux values from observed meteorological conditions. For each hindcast, the INTERP meteorological data interpolation program, written by Dr. David Schwab of NOAA GLERL, Ann Arbor, was first used to convert the temporally and spatially disparate meteorological point data in the NOAA CoastWatch Marine Observations (MAROBS) data stream into hourly fields of interpolated air temperature, dew point, cloud cover, and wind components that match the Lake Michigan computational grid. INTERP adjusts all wind observations to 10 m above water level, based on stability theory, and accounts for the effect of overland to oversea roughness differences on

winds. These adjustments are documented in Schwab and Morton (1984). The stability adjustments require a water surface temperature; a lakewide mean value was calculated from observations when possible, with a long term mean value for Lake Michigan on the particular Julian day used as a backup. The interpolated meteorological fields were read in hourly by CH3D and used in subroutine SOLAR, written by Dr. Michael McCormick of NOAA GLERL, to calculate the incoming solar radiation, based on the work of Cotton (1979). A new subroutine, HEATFLUX, based on the theory of Edinger et al. (1974), was then used to calculate the surface heat exchange coefficient, K, and the equilibrium temperature, T_e, at each grid point from the local solar radiation, dew point, wind speed, and CH3D water surface temperature, T. The CH3D water surface temperature boundary condition is then (Chapman et al., 1996)

$$\frac{\partial T}{\partial z} = \frac{\mathrm{Pr}_V}{E_V} K(T - T_e), \tag{3}$$

where z is the vertical co-ordinate, Pr_V is the vertical Prandtl number (equal to the ratio of the vertical eddy viscosity A_V to vertical eddy diffusivity K_V), and E_V is the vertical Ekman number (the non-dimensional reciprocal of the Coriolis force). The initial water temperature throughout the lake was set to 1.1 $^\circ$C, the long term mean value for Julian day 86. The interpolated and adjusted hourly wind fields generated by the INTERP program were also used as WAM inputs in the EEGLE hindcasts.

For the period Julian day 86 – 99, sets of 24-hour hindcasts were run for no coupling, one-way coupling (each model reads the required arrays every hour from files generated by the other model's no coupling run), and two-way coupling with 60 minute and 3 minute coupling time-steps.

Figure 3 shows contours and vectors of WAM significant wave heights at hour-78 of the no-coupling hindcast. The axis scales refer to the Lake Michigan computational grid; a 3 minutes longitude by 2 minutes latitude grid (approximately 4-km square cells) was used. The maximum significant wave height, in meters, and its grid cell location are indicated in the figure. At hour-78 the winds were predominantly from the south and this is reflected in the wave directions. Wind speeds were on the order of 12 m/s, but were stronger in the north and south of the lake than in the center; this explains the distribution of wave heights. Figure 4 shows CH3D surface current vectors and water elevation contours at hour-78 of the no-coupling hindcast. The maximum surface current and its location are indicated. In figure 4 the southerly wind has caused a storm surge in the north of the lake. Figure 5 shows the CH3D predictions at hour-78 for two-way coupling every 3 minutes. Comparing figures 4 and 5 it can be seen that the interactions with the wave fields have significantly increased the CH3D storm surge, the associated drawdown in the south of the lake, and the surface currents in general. Figure 6 shows WAM wave predictions at hour-78 of the two-way coupling, 3-minute coupling time-step hindcast. Comparing figures 3 and 6 shows that the current effects in WAM have slightly reduced the wave heights. This is due to a reduction in the effective wind speed.

Figure 7 shows WAM wave predictions at hour-216 of the no coupling hindcast. At hour-216 winds were predominantly from the north, with a typical magnitude of 10 m/s. This resulted in

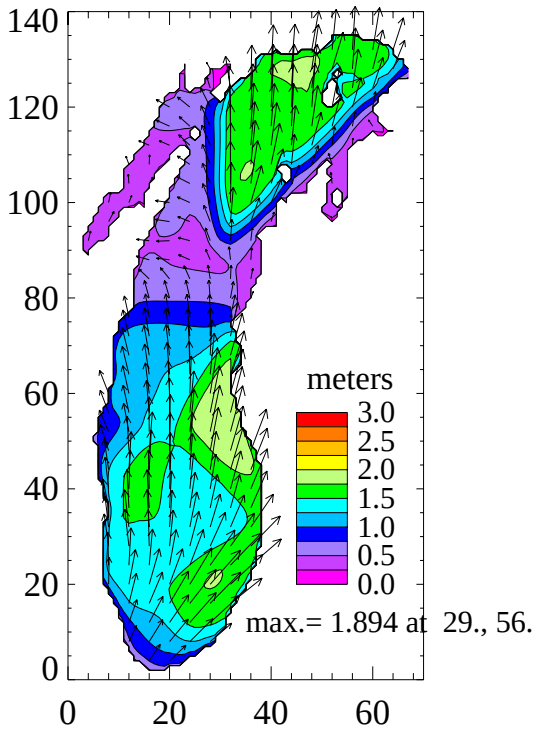

Figure 3: WAM wave heights at hour-78 of EEGLE hindcast for no coupling

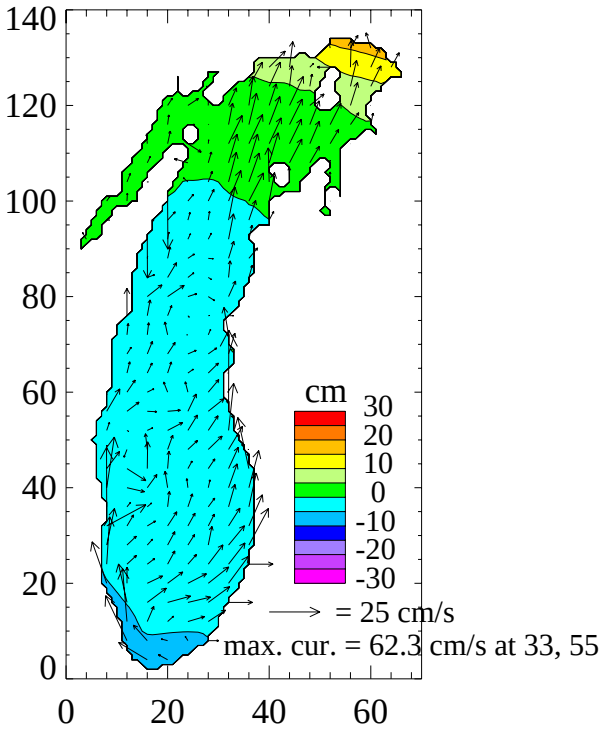

Figure 4: CH3D surface currents and elevations at hour-78 of EEGLE hindcast for no coupling

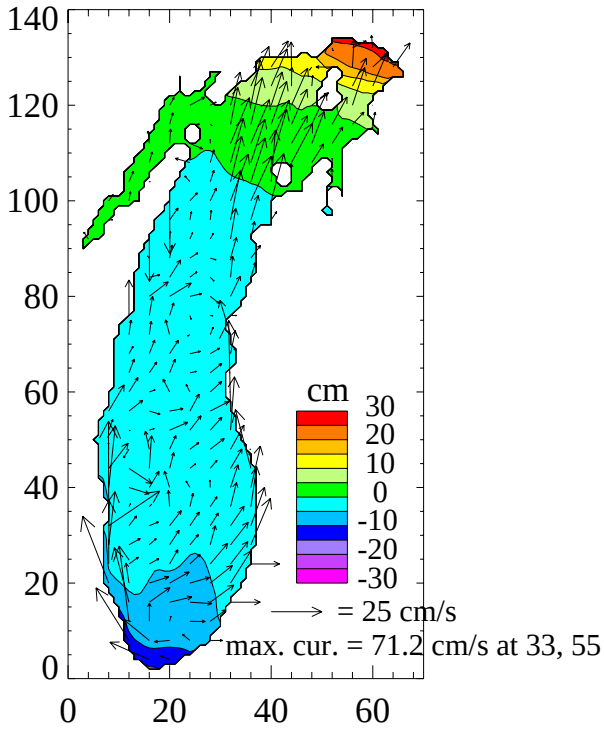

Figure 5: CH3D surface currents and elevations at hour-78 of EEGLE hindcast for two-way coupling every 3 minutes

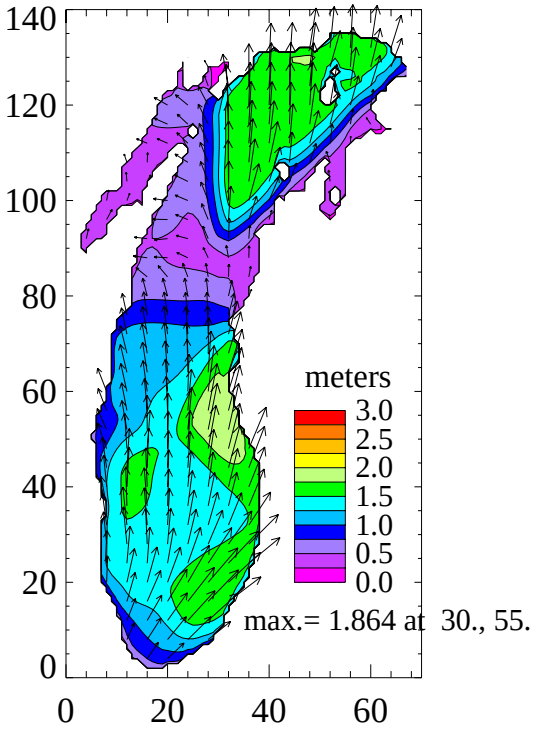

Figure 6: WAM wave heights at hour-78 of EEGLE hindcast for two-way coupling every 3 minutes

fetch-limited wave growth over most of the lake, with the maximum wave height occurring close to the southern shore, as shown in the figure. Figure 8 shows CH3D surface current and water elevation predictions at hour-216 of the no-coupling hindcast. In this case the storm surge occurs in the south of the lake, along with the highest surface currents. Figures 9 and 10 show the CH3D predictions at hour-216 of the two-way coupling hindcasts with coupling time-steps of 60 minutes and 3 minutes, respectively. Comparing these figures with figure 8 shows that the wave effects again cause an enhanced surge and increased currents. It can also be seen that the coarser coupling time-step results in the greatest surge and currents. The reason for this is that the infrequent feedback between the two models' wave-current interactions in the 60-minute coupling run results in an overshoot of the coupling effects. When wave effects increase currents, the increased currents (which transport the waves) reduce the relative motion of the waves and the wind. This reduces the effective wind speed, slowing wave growth. This in turn decreases the wave effects on the currents, setting up a feedback mechanism. With the 60-minute coupling, the feedback is clearly not permitted often enough. Figures 11 and 12 show the WAM predictions at hour-216 for the 60-minute and 3-minute coupling time-steps, respectively. Comparing these figures with figure 7, one can see that the current effects reduce the wave heights, as at hour-78. There is also further evidence that the coarser coupling time-step results in an overprediction of the coupling effects. Results are not shown for the one-way coupling hindcast, but in that case the overprediction of the coupling effects was larger than in the coarse two-way coupling hindcast. This is to be expected since there is no feedback between the two models' coupling effects.

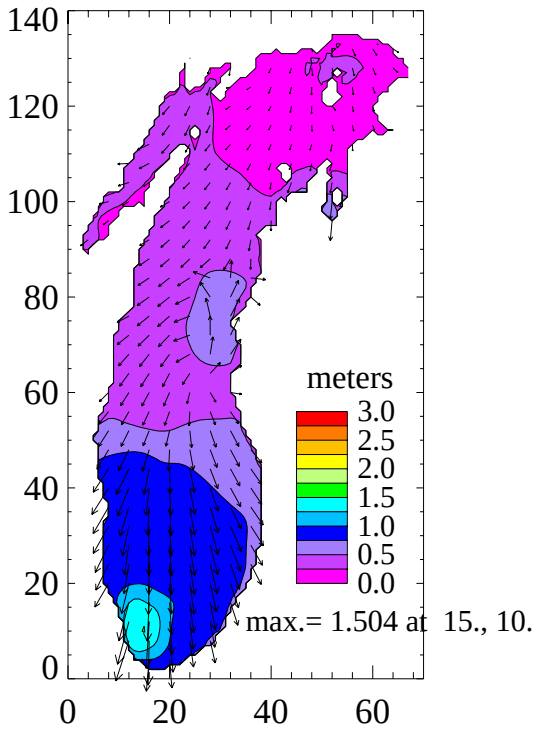

Figure 7: WAM wave heights at hour-216 of EEGLE hindcast for no coupling

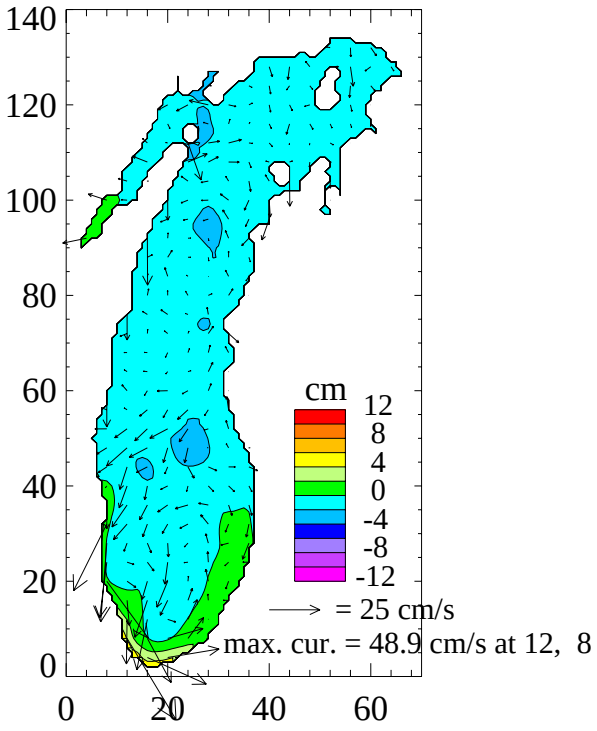

Figure 8: CH3D surface currents and elevations at hour-216 of EEGLE hindcast for no coupling

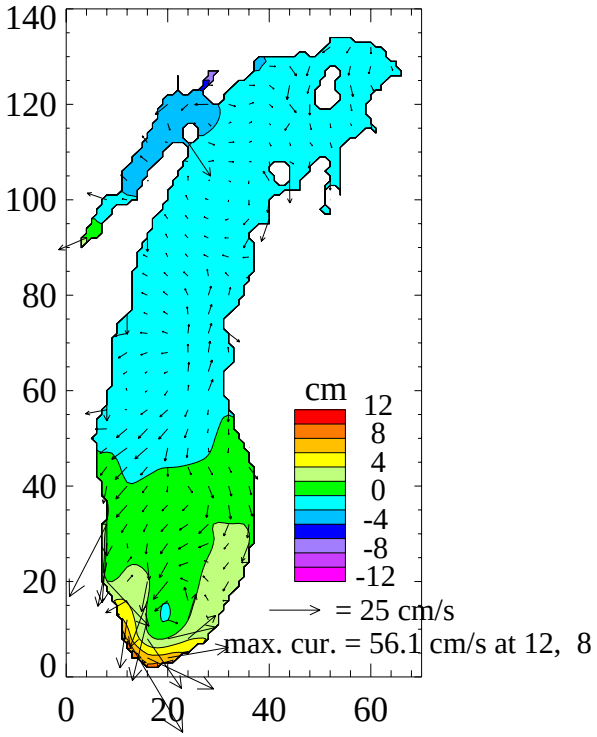

Figure 9: CH3D surface currents and elevations at hour-216 of EEGLE hindcast for two-way coupling every 60 minutes

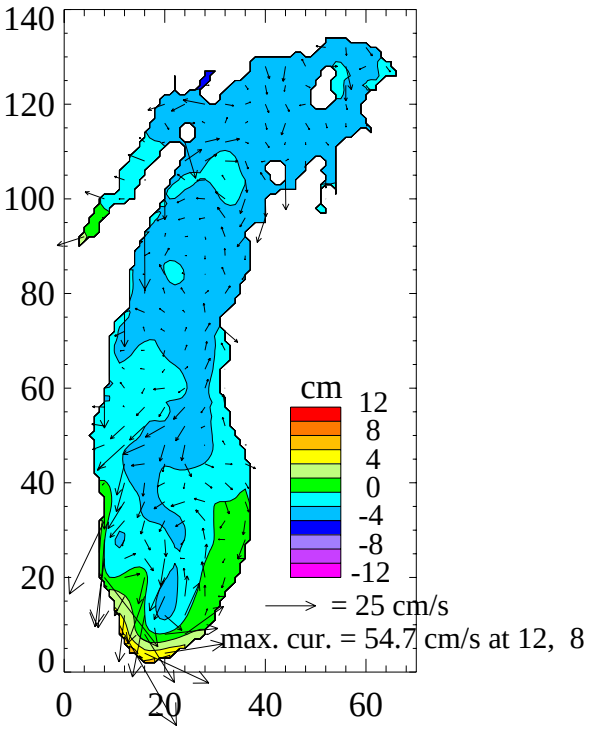

Figure 10: CH3D surface currents and elevations at hour-216 of EEGLE hindcast for two-way coupling every 3 minutes

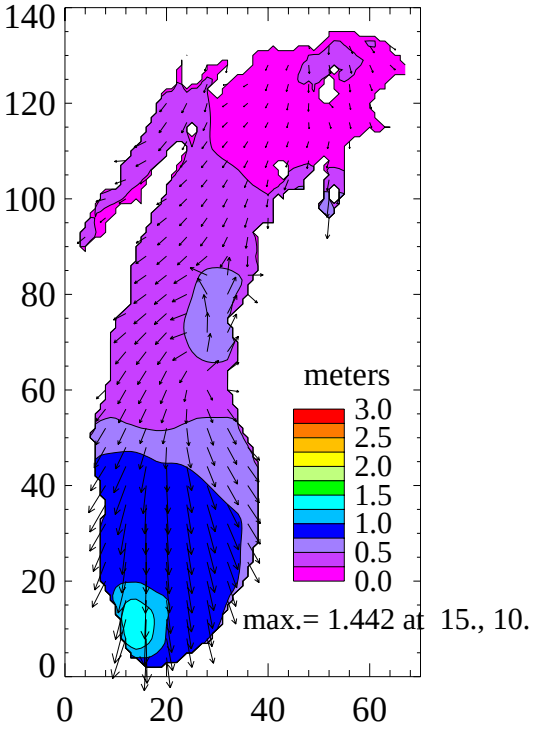

Figure 11: WAM wave heights at hour-216 of EEGLE hindcast for two-way coupling every 60 minutes

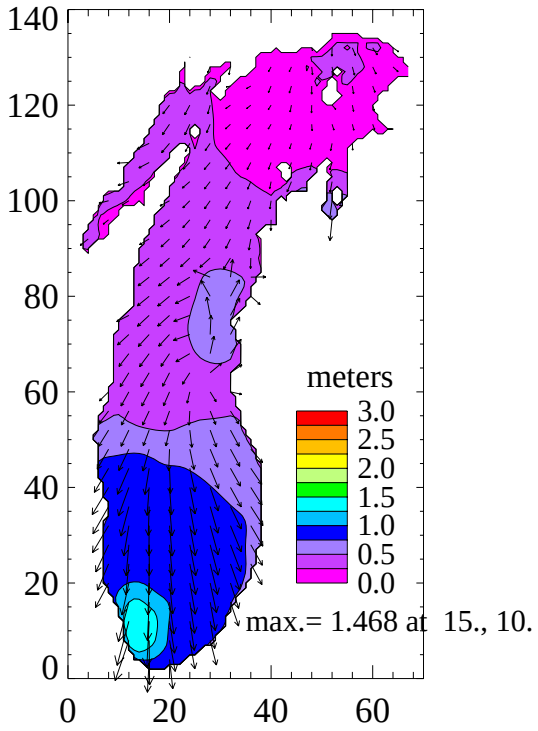

Figure 12: WAM wave heights at hour-216 of EEGLE hindcast for two-way coupling every 3 minutes

In general the Lake Michigan EEGLE hindcasts indicated that coupling increases CH3D storm surges and surface currents on the order of 20 %. In continental shelf waters this would translate to increased surges on the order of several feet, which could greatly influence the planning of military operations. The coupling effects in WAM typically modified wave heights on the order of 3 %, but impact would be greater in high current regions such as the Gulf Stream. One-way coupling overpredicted coupling effects on the order of 25 % and two-way coupling only every 60 minutes overpredicted effects on the order of 10 %.

The hindcast predictions of water elevations and wave heights were compared with data. The coupling effects noticeably affected how predicted time series matched with observations, but there was no conclusive proof that the coupled hindcast predictions were more accurate. The reasons for this were the low “signal to noise” ratios. The coupling effects on waves were small, and while the coupling effects on storm surges were significant, the surges themselves were relatively small. Furthermore, the circulation patterns in some of the interpolated wind fields used to drive the hindcasts were clearly unrealistic. Future hindcasts should model a location where storm surges are on the order of meters and should use wind fields from meteorological simulations.

2.5 Scalability of the coupled system and individual models

The scalability of the coupled CH3D/WAM system and the individual parallel codes has been measured. Wallclock timings were recorded for 24-hour simulations using the 4-km Lake Michigan grid. It was found that the time required for an OpenMP WAM run was equal to the

time required for a coupled run involving the same number of WAM threads. Furthermore, the number of CH3D processes used in a coupled run was found to have no effect on the time required. The explanation for these results is that the WAM model is far more computationally demanding than the CH3D model.

Figure 13 shows the scalability of the coupled system on the O2K platform. As explained above, this figure also indicates the scalability of stand-alone WAM runs and the number of CH3D processes is not important. It can be seen that the reduction in execution time levels off around 8

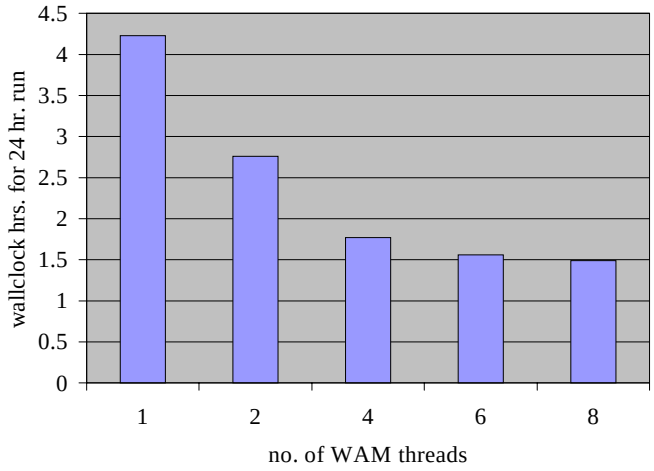

Figure 13: Scalability of coupled CH3D/WAM on the O2K for the 4-km Lake Michigan grid

WAM threads. This is partly due to the relatively small number of computational cells in the Lake Michigan grid, but this cannot be the only cause since the scalability of the parallel CH3D model extends further on the same grid (see below). Another factor inhibiting coupled system scalability is that due to time constraints, efficient OpenMP directives were established for only the four most demanding WAM subroutines. As stated in section 2.1, parallelization of the remainder of the code was achieved using the PFA compilation argument, which sometimes implements parallel directives that actually slow down execution.

The scalability of the parallel CH3D model is shown in figures 14 and 15, for the O2K and T3E platforms, respectively. It can be seen that for both platforms execution speed-up levels off in the vicinity of 32 processors. In this case the small size of the Lake Michigan grid is the sole cause of the limit. The grid has 67 columns, 139 rows, and 3932 water cells. This means that for 32 processors, the domain decomposition strategy in CH3D (refer to section 2.1) results in each processor performing calculations for typically 4 rows and 120 cells. For such small blocks, the MPI communication overhead becomes significant and offsets the benefit of further increasing the number of processors. The scalability of the CH3D model would extend well above 32 processors in deployments involving a larger computational grid.

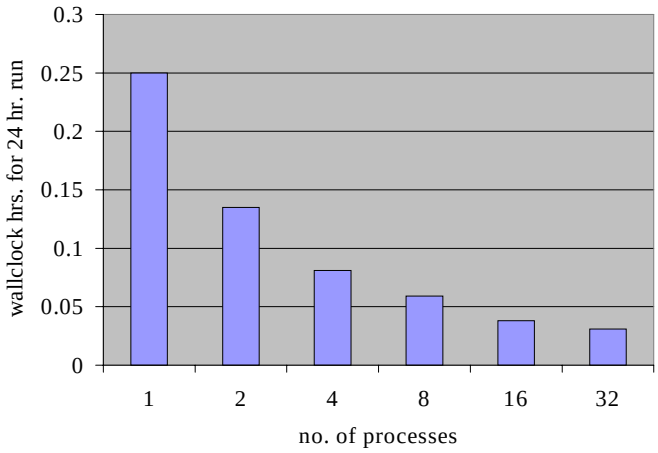

Figure 14: Scalability of the parallel CH3D model on the O2K for the 4-km Lake Michigan grid

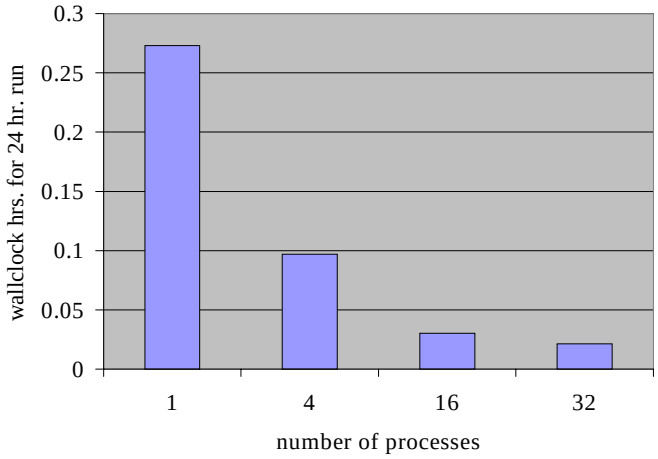

Figure 15: Scalability of the parallel CH3D model on the T3E for the 4-km Lake Michigan grid

3. Coupling at the bottom boundary layer

3.1 Motivation

The marine bottom boundary layer has significant effects on current and wave conditions. Both motions lose energy through contact with bed particles and bedforms. In addition, suspended sediment can cause density gradients and the damping of turbulence, both of which influence current patterns. Both wave and current motions cause a bottom boundary layer; by definition, the layer is the vertical distance within which bottom drag causes far field velocities to be reduced by a specific percentage, typically 1 %. Theory and observations have shown (Grant and Madsen, 1979; Keen and Slingerland, 1993) that a wave boundary layer and a current boundary layer do not combine in a linear manner. Each field of motion is therefore affected by the other's boundary layer, when it is significant. This interaction has traditionally been neglected, with

wind waves and marine circulation normally modeled independently. This can cause sizable errors, particularly in shallow water when significant wave-induced orbital motion extends to the bed.

In this focused effort the marine bottom boundary layer is more realistically represented by the coupling of the WAM wave model (WAMDI, 1988) and the CH3D-SED marine circulation and sediment transport model (Spasojevic and Holly, 1994). The resulting improved sediment transport predictions will benefit navigation channel dredging activities and the identification of suspended sediment clouds in which hostile or friendly submarine craft might position themselves to avoid detection by sonar. More accurate bottom conditions should also improve the wave and circulation predictions of the coupled WAM/CH3D-SED system, aiding the planning of military operations such as amphibious landings, ship routing, and search and rescue.

3.2 WAM and CH3D-SED bottom boundary layers

Descriptions of the WAM and CH3D models are contained in section 2 of this report. The bottom boundary layer representations of WAM and CH3D-SED are detailed in this section. CH3D-SED is an extension of the basic CH3D model, with the SED sediment transport sub-model fully integrated with circulation calculations.

Equation (1), above, is the parameterization used in WAM for the dissipation of wave energy by bottom friction (Collins and Hasselmann, 1972. In (1), 0.076 is the value of the drag coefficient, C_d . The value of C_d is selected to suit the model's deployment location, but the lack of spatial and temporal variation will obviously cause errors in the calculation of $S_{bf}(\omega,\theta)$ rates.

The SED sub-model in CH3D-SED models erosion, deposition, bedload transport, and suspended sediment transport for a number of user-specified sediment size classes. The particle size and density are specified for each class, along with initial and boundary conditions for bed and suspended sediment concentrations. Each time-step, CH3D supplies SED with grids of water depth and current. SED returns grids of bottom roughness, modified water depth, and the near-bottom water/sediment mixture density.

The SED model is based on the concept of an active layer at the top of the bed in which erosion, deposition, and bedload transport occur. The conservation of mass for a particular size class in the active layer is given by

$$\rho_s(1-p)\frac{\partial(\beta E_{m)}}{\partial t}+\tilde{\nabla}\cdot\tilde{q}_b+S_e-S_d-S_F=0, \qquad (4)$$

where ρ_s is the sediment density, p is the bed porosity, β is the size fraction by mass, E_m is the active layer thickness, $\tilde{q}_b$ is the bedload flux vector, S_e is the erosion sink term (movement of active layer particles into suspension), S_d is the deposition source term, and S_F represents the exchange of particles between the active layer and the strata below.

The erosion term is parameterized as

$$S_e = -\beta_2 \left(D_V \frac{\partial(\rho_m C)}{\partial z} \right)_{z=a}, \tag{5}$$

where β_2 represents an availability factor for the size class, D_V is the vertical diffusivity for sediment, ρ_m is the total density of the sediment/water mixture, C is the concentration for the size class, and a is a near-bed reference elevation. The deposition term is parameterized as

$$S_d = \left(w_f \rho_m C \right)_{z=a+\Delta a}, \tag{6}$$

where w_f is the settling velocity. The cross-layer exchange term is parameterized as

$$S_F = \rho_s'(1-p) \frac{\partial}{\partial t} \left[\beta' \left(E_m - z_b \right) \right], \tag{7}$$

where the primed parameters are for the same size class below the active layer, and z_b is bed elevation.

Integrating (4) over all n size classes ($\sum \beta = \sum \beta' = 1$), using (7), and assuming constant ρ_s then gives an equation for the conservation of all active layer sediment:

$$\rho_s (1-p) \frac{\partial z_b}{\partial t} + \sum_n \left(\tilde{\nabla} \cdot \tilde{q}_b + S_e - S_d \right) = 0. \tag{8}$$

SED conserves suspended sediment mass for each size class at each sigma layer using

$$\frac{\partial(\rho_m C)}{\partial t} + \frac{\partial(\rho_m C u)}{\partial x} + \frac{\partial(\rho_m C v)}{\partial y} + \frac{\partial(\rho_m C w)}{\partial z} - \frac{\partial\left(\rho_m C w_f\right)}{\partial z} = \frac{\partial}{\partial x}\left[D_H \frac{\partial(\rho_m C)}{\partial x} \right] + \frac{\partial}{\partial y}\left[D_H \frac{\partial(\rho_m C)}{\partial y} \right] + \frac{\partial}{\partial z}\left[D_V \frac{\partial(\rho_m C)}{\partial z} \right], \tag{9}$$

where u, v, and w are the CH3D current components for the sigma layer, D_V is as above, and D_H is the horizontal diffusivity for sediment.

The set of equations (4) – (9) contain several unknown quantities. To permit a solution, the primary unknowns are selected as z_b, the modified β and β' values, and the C values. The remaining unknowns are parameterized using expressions called auxiliary relations. These are given by (10) - (13):

$$C_a = 0.015 \frac{D}{a} \frac{T_*^{1.5}}{D_*^{0.3}}, \tag{10}$$

where a is a user-input estimate of half the bed ripple height, D is the sediment particle diameter, D_* is the nondimensional diameter = $Fn\left[D, \frac{\rho_s}{\rho}, \nu\right]$, ν is kinematic viscosity, T_* is a nondimensional transport mode parameter = $Fn\left[u_*, u_{*crit}\right]$, u_* is the nondimensional effective bed shear velocity, and u_{*crit} is a critical value for the onset of motion, found from Shields' diagram.

$$q_b = 0.053\rho_s\left[\left(\frac{\rho_s}{\rho}-1\right)gD\right]^{1/2}\frac{T_*^{2.1}}{D_*^{0.3}}D, \tag{11}$$

where g is gravitational acceleration.

$$w_f = Fn\left[\frac{\rho_s}{\rho}, D, \nu\right], \tag{12}$$

$$D_V = \beta_3\phi A_V, \tag{13}$$

where ϕ is a function of C_a and represents the damping of turbulence by sediment, A_V is the CH3D vertical diffusivity for water particles, and $\beta_3 = Fn\left[\omega_f, u_*\right]$, quantifying the difference in the diffusion of sediment particles versus water particles. D_H is set to a constant value input by the user.

SED uses an implicit numerical scheme that is forward in time and centered in space. The same horizontal grid is used as in CH3D. The solution procedure each time-step is:

1. simultaneously solve (8) and (4) for each sediment class; this gives β, β', and z_b predictions
2. solve (9) for each size class, one at a time, for each sigma layer; this gives $C(z)$ predictions
3. iterate steps 1 and 2 until convergence criteria are met
4. repeat steps 1 to 3 across the horizontal grid

3.3 Combined wave-current boundary layer

The many assumptions inherent in the SED auxiliary relations (10) - (13) introduce errors. Furthermore, the model does not account for the effects of a co-existing wave field on sediment transport. For these reasons, this focused effort has targeted the replacement of (10) - (13) with a more sophisticated treatment based on the combined wave-current boundary layer work of Grant and Madsen (1979), as extended by Keen and Glenn (1998).

The wave-current boundary layer of Grant and Madsen (1979) was designed for wave-dominated conditions and did not account for stratification due to suspended sediment. The stratification

effect was added by Glenn and Grant (1987). Keen and Glenn (1994) modified the Grant and Madsen (1979) theory to extend applicability to a wide range of wave-current conditions. Keen and Glenn (1998) added the modifications of Keen and Glenn (1994) to the theory of Glenn and Grant (1987). They coupled their boundary layer model with an ocean circulation model and used hindcast wind and wave fields in the simulation of the ocean response to Hurricane Andrew off the coast of Louisiana.

In a typical combined boundary layer, the wave boundary layer is embedded within the lower portion of the current boundary layer. This occurs because the height of a boundary layer caused by a wave-induced orbital velocity is much less than that of a boundary layer caused by an equivalent current. As a result, the wave boundary layer causes relatively large stresses over a short vertical distance. This increases the turbulent diffusion of fluid close to the bed, which causes the current boundary layer to experience an increased bottom roughness. The suspended sediment stratification correction has an opposing effect; the stratification reduces turbulent diffusion, therefore reducing bottom roughness.

The wave-current boundary layer code used in this research is a new sub-model named BBL. The main purpose of BBL is to supply SED with more accurate predictions of the parameters previously calculated using the SED auxiliary relations, and therefore permit improved prediction of sediment transport and concentration. BBL can also supply CH3D and WAM with temporally and spatially varied, more accurate bottom friction coefficients. The final product is a coupled system of codes with a realistic representation of the bottom boundary layer, resulting in improved predictions in each component model.

The BBL model uses two dimensionless shear velocities that represent the interacting effects of the wave and current boundary layers. The maximum combined shear velocity is given by

$$u_{*_{cw}} = \left[\frac{1}{2} f_{cw} u_b^2 \alpha\right]^{1/2}, \tag{14}$$

where u_b is the wave-induced orbital velocity at the top of the wave boundary layer, α is a dimensionless function that accounts for current effects (Keen and Glenn, 1994), and f_{cw} is a combined wave-current friction factor calculated from a nonlinear, directional function of u_b, the near-bed current, and parameters describing the sediment size classes. The time-averaged shear velocity is given by

$$u_{*_c} = \left[\frac{1}{2} f_{cw} u_b^2 V_2\right]^{1/2}, \tag{15}$$

where V_2 is another dimensionless function, similar to α in (14), first used in Grant and Madsen (1979). $u_{*_{cw}}$ and u_{*_c} essentially correspond to wave and current effects, respectively, with f_{cw}, α, and V_2 accounting for the interactions between the boundary layers. The height of the wave boundary layer, at which u_b is required, is taken as

$$\delta_w = \frac{2\kappa u_{*_{cw}}}{\omega}, \tag{16}$$

where κ is the von Karman coefficient, (= 0.4), and ω is a representative radian wave frequency, taken here to be the peak wave frequency. It should be noted that (14) and (15) are similar in form to the widely used Taylor drag law:

$$\tau = \left[C_d u^2\right]^{1/2}, \tag{17}$$

where τ represents shear stress, C_d is a drag coefficient, and u is a velocity.

BBL uses (14) – (16) in the calculation of the apparent bottom roughness due to the combined boundary layer:

$$k_{bc} = k_b \left[30 \frac{\delta_w}{k_b} \right]^{\left(1 - \frac{u_{*_c}}{u_{*_{cw}}}\right)}, \tag{18}$$

$$= k_b \left[30 \frac{\delta_w}{k_b} \right]^{\left(1 - \left(\frac{V_2}{\alpha}\right)^{1/2}\right)}, \tag{19}$$

where k_b is the physical bottom roughness and

$$k_b = k_{bR} + k_{bT}, \tag{20}$$

with k_{bR} related to ripple height and steepness and k_{bT} related to the thickness of the active sediment transport layer. BBL calculates k_{bR} and k_{bT} using the near-bottom current velocity and the sediment size class parameters; these calculations are based on the moveable bed roughness theory of Grant and Madsen (1982). For large waves and small currents, function $V_2 \to 0$, while function $\alpha \to 1$. This means that (19) gives $k_{bc} \approx 30\delta_w$, which is the strictly wave boundary layer roughness. Conversely, for small waves and large currents, the ratio $V_2 / \alpha \to 1$, and k_{bc} from (19) reverts to the current boundary layer roughness, k_b.

The current profile for the combined boundary layer is given by

$$u(z) = \frac{u_{*_c}}{\kappa} \left(\ln \frac{30z}{k_{bc}} + \beta\alpha \ln \frac{z}{\delta_w} \right). \tag{21}$$

The solution procedure in BBL is:

1. calculate reference current u_a using the unstratified wave-current boundary layer theory of Keen and Glenn (1994); this is used as a first guess for reference current $u(z_r)$, where z_r is taken as 1 m
2. evaluate functions V_2 and α and calculate θ_{cw}, the angle between the current and wave velocity vectors
3. estimate f_{cw}, then $u_{*_{cw}}$ and u_{*_c}, using (14), (15), and additional equations from Keen and Glenn (1998)
4. estimate k_b using (20) and additional equations from Grant and Madsen (1982)
5. estimate k_{bc} using (18)
6. estimate $u(z_r)$ using (21)
7. return to step 2 and iterate until $u(z_r)$ convergence meets the required criteria

The BBL model requires inputs from each of the other models in the coupled system, and supplies them with outputs. The links are as follows:

- from CH3D to BBL:
  - u_r, the current at reference elevation z_r = 1 m; this requires interpolation between sigma layers
  - θ_{cr}, the current direction at reference elevation z_r

- from SED to BBL:
  - D, the sediment particle diameter
  - ρ_s, the sediment density
  - w_f, the settling velocity
  - C_b, the active layer concentration
  - $u_{*_{crit}}$, the critical nondimensional shear velocity for the onset of motion, from Shields' diagram
  - E_m, the active layer thickness
  - ξ, a representative ripple height
  - ξ/λ, a representative ripple steepness; λ = a representative ripple wavelength

- from WAM to BBL:
  - u_b, the wave-induced orbital velocity at the bed
  - A_b, the maximum horizontal excursion due to u_b
  - θ_w, the mean wave direction

- from BBL to CH3D:
  - k_{bc}, the bottom roughness for the combined boundary layer

- from BBL to SED:

- $u_{*_{cw}}$, the nondimensional shear velocity for the combined boundary layer
- f_{cw}, the bottom friction coefficient for the combined boundary layer
- k_{bc}, the bottom roughness for the combined boundary layer

- from BBL to WAM:
  - f_{cw}, the bottom friction coefficient for the combined boundary layer

3.4 Accomplishments

In PET year 3 the coupling of CH3D-SED and WAM at the bottom boundary layer has been completed in a one-way coupled, sequential form, using the 4-km Lake Michigan grid. In this version the WAM inputs required in BBL are read from files generated by a stand-alone WAM run. Preliminary analysis of an idealized test case indicates that the implementation of the wave-current boundary layer significantly affects the sediment predictions of CH3D-SED in the nearshore zone.

The two-way coupled CH3D-SED/WAM/BBL system will be built in PET year 4 using parallel versions of the codes. In preparation for this work, the CH3D-SED model was parallelized in year 3. Full details of the parallelization strategy, verification of the parallelization, test results, and scalability are given in Bangalore et al. (1999).

4. Conclusions

This focused effort entailed the coupling of marine circulation and wind-wave models that are frequently used by CEWES MSRC scientists. Parallel versions of the CH3D circulation model and the WAM wave model were coupled at the atmospheric boundary layer using the MPI library. The parallelizations of the codes were first verified and it was found that the MPI-based parallel WAM code contained errors related to shallow water current effects and grid nesting. It was therefore replaced in this project by an OpenMP version of WAM. This restricts WAM runs to the SGI ORIGIN 2000 platform until OpenMP is ported to other parallel machines. Cross-platform coupling is possible through use of the MPI_Connect library. During the testing of WAM, sign errors were also found in the main propagation subroutine. These errors were corrected, resulting in realistic current-induced refraction predictions.

Lake Michigan hindcasts were performed to evaluate the importance and accuracy of the model coupling. In the hindcasts, coupling effects increased storm surges and surface currents on the order of 20 %, and reduced wave heights on the order of 3 %. It was also found that frequent passing of arrays between the models was required. For a coarse coupling time-step of 60 minutes, coupling effects were overpredicted on the order of 10 % in comparison with coupling every 3 minutes. If one-way coupling was used, the overprediction rose to 25 %. Comparisons were made between predicted and observed water elevations, but the results were inconclusive due to the relatively small Lake Michigan storm surges and the large errors in the interpolated wind fields used to drive the hindcasts. It was concluded that future evaluations should use wind fields from meteorological models and a test location where surges are larger. It would also be beneficial to select a location of strategic importance to the military.

The scalability of the coupled system and the component models was measured. The WAM model is far more computationally demanding than CH3D and the time required for a coupled run was found to equal to the time required for a stand-alone WAM run with the same number of threads. Speed-up of the coupled simulations leveled off at 8 WAM threads. This was partly related to the small computational grid, but also due to time constraints limiting optimized implementation of OpenMP to the four most demanding WAM subroutines. The CH3D model reached a minimum execution time at 32 processors, with this limit due solely to the size of the Lake Michigan grid.

The CH3D-SED circulation and sediment model and the WAM model were coupled at the bottom boundary layer. The representation of the bottom boundary layer in the SED sediment transport and suspension sub-model does not account for wave effects and also uses some basic parameterizations that are simplistic and inaccurate. The coupling was achieved using the new BBL sub-model, which receives inputs from CH3D-SED and WAM, models a realistic combined wave-current boundary layer, then returns bottom roughnesses, friction coefficients, and shear velocities to CH3D-SED and WAM. The inaccurate parameterizations in SED are no longer required. One-way coupling of sequential versions of the codes has been completed, with the WAM inputs to BBL read from file. A parallel version of CH3D-SED is now available and a two-way coupled, parallel version of the CH3D-SED/WAM/BBL system will be built in the coming year.

Coupling at the atmospheric boundary layer improves predictions of water levels, currents, and wave heights, which are important factors in planning military operations such as beach landings, fleet navigation, and search and rescue. Coupling at the bottom boundary layer improves the prediction of suspended sediment clouds, which can be used in the concealment of submarine craft. A better representation of the bottom boundary layer also aids circulation and wave prediction. In the future it would be highly beneficial to incorporate an atmospheric circulation model into the scaleable, coupled system. The inaccuracies in the Lake Michigan storm surge predictions indicate the importance of having accurate wind fields to drive the coupled system. Research has also shown that couplings between winds and surface currents and winds and waves can greatly affect each field of motion.

The use of parallel codes permits mission critical forecasts to be generated more quickly and/or at a higher resolution. These advantages show the significant impact of the availability of high performance computing facilities at the CEWES MSRC.

Acknowledgement

This work was supported in part by a grant of HPC time from the DoD HPC Modernization Program.

References

Bangalore, P. V., Zhu, J., Huddleston, D., Skjellum, A., Welsh, D. J. S., Bedford, K. W., Wang, R. and Sadayappan, P. (1999). Parallelization of a coupled hydraulics and sediment transport model, *CEWES MSRC PET Technical Report*, Mississippi State University and The Ohio State University. Prepared for the Department of Defense HPC Modernization Program.

Bova, S. W., Breshears, C. P., Cuicchi, C., Demirbilek, Z. and Gabb, H. A. (1999). Dual-level parallel analysis of harbor wave response using MPI and OpenMP, submitted to *International Journal of High Performance Computing Applications*.

Chapman, R. S., Johnson, B. H. and Vemulakonda, S. R. (1996). User's guide for the sigma stretched version of CH3D-WES; a three-dimensional numerical hydrodynamic and temperature model, *Technical Report HL-96-21*, U.S. Army Engineer Waterways Experiment Station, Vicksburg, MS.

Cotton, G. F. (1979). ARL models of global solar radiation, in *Hourly Solar Radiation – Surface Meteorological Observations. Solmet, Volume 2, Final Report*, National Climate Center, Department of Energy.

Edinger, J. E., Brady, D. K. and Geyer, J. C. (1974). Heat exchange and transport in the environent, *Electric Power Research Institute publication no. 74-049-00-3*, EPRI, Palo Alto, CA.

Glenn, S. M. and Grant, W. D. (1987). A suspended sediment stratification correction for combined wave and current flows, *Journal of Geophysical Research* **92**: 8244—8264.

Grant, W. D. and Madsen, O. S. (1979). Combined wave and current interaction with a rough bottom, *Journal of Geophysical Research*, **84**: 1797-1808.

Grant, W. D. and Madsen, O. S. (1982). Moveable bed roughness in unsteady oscillatory flow, *Journal of Geophysical Research*, **87**: 469-481.

Gunther, H., Hasselmann, S. and Janssen, P. A. E. M. (1992). The WAM model cycle 4, *Technical Report*, Deutsches KlimaRechenZentrum, Hamburg, Germany.

Hasselmann, K., Barnett, T. P., Bouws, E., Carlson, H., Cartright, D. C., Enke, K., Ewing, J., Gienapp, H., Hasselmann, D. E., Kruseman, P., Meerburg, A., Muller, P., Olbers, D. J., Richter, K., Sell, W. and Walden, H. (1973). Measurements of wind-wave growth and swell decay during the Joint North Sea Wave Project (JONSWAP), *Deutsches Hydrographisches Z.* **8**(12), Supplement A.

Holthuijsen, L. H. and Tolman, H.L. (1991). Effects of the Gulf Stream on ocean waves, *Journal of Geophysical Research* **96**: 12755-12771.

Keen, T. R. and Glenn, S. M. (1994). A coupled hydrodynamic-bottom boundary layer model of Ekman flow on stratified continental shelves, *Journal of Physical Oceanography* **24**: 1732-1749.

Keen, T. R. and Glenn, S. M. (1998). Resuspension and advection of sediment during Hurricane Andrew on the Louisiana continental shelf, *Proceedings of the 5th International Conference on Estuarine and Coastal Modeling*, 481-494.

Keen, T. R. and Slingerland, R. L. (1993). A numerical study of sediment transport and event bed genesis during Tropical Storm Delia, *Journal of Geophysical Research* **98**: 4775-4791.

Komen, G. J., Cavalieri, L., Donelan, M., Hasselmann, K., Hasselmann, S. and Janssen, P. A. E. M. (1994). *Dynamics and Modelling of Ocean Waves*, Cambridge University Press, Cambridge, U.K.

Phillips, O. M. (1977). The sea surface, *Modelling and Prediction of the Upper Layers of the Ocean*, Pergamon Press, Elmsford, NY, pp. 229-237.

Schwab, D. J., Beletsky, D., and Lou, J. (1999). The 1998 coastal turbidity plume in Lake Michigan, *Estuarine, Coastal and Shelf Science*, in press.

Schwab, D. J. and Morton J. A. (1984). Estimation of overlake wind speed from overland wind speed: a comparison of three methods, *Journal of Great Lakes Research* **10**: 68-72.

Spasojevic, M. and Holly, M. J. (1994). Three dimensional numerical simulation of mobile-bed hydrodynamics, *Technical Report HL-94-2*, U.S. Army Engineer Waterways Experiment Station, Vicksburg, MS.

WAMDI (1988). The WAM model – a third generation ocean wave prediction model, *Journal of Physical Oceanography* **18**: 1775-1810.

Zhang, S., Welsh, D., Bedford, K., Sadayappan, P. and O'Neill, S. (1998). Coupling of circulation, wave and sediment models, *Technical Report CEWES MSRC/PET TR/98-15*, The Ohio State University, Columbus, OH. Prepared for the Department of Defense HPC Modernization Program.